Ab Initio Reaction Path Analysis for the Initial Hydrogen Abstraction from Organic Acids by Hydroxyl Radicals

Wenjie Sun,[†] Liming Yang,[‡] Liya Yu,[‡] and Mark Saeys*,[†]

Department of Chemical and Biomolecular Engineering, 4 Engineering Drive 4, National University of Singapore, Singapore 117576, Division of Environmental Science and Engineering, 9 Engineering Drive 1, National University of Singapore, Singapore 117576

Received: October 14, 2008; Revised Manuscript Received: May 5, 2009

Hydrogen abstraction from organic acids by hydroxyl radicals is the initial rate- and selectivity-determining step in the photochemical oxidation of organic acids in the troposphere. To quantify the rate and selectivity of these reactions, the abstraction of hydrogen atoms at the acid, α, β, γ, and methyl positions was studied for valeric acid, C_4H_9COOH, using first principles calculations. At the high-pressure limit, an overall rate coefficient at 298 K of 4.3×10^6 m^3/(mol s) was calculated. The dominant pathways are abstraction at the β; the γ; and, to a lesser extent, the acid positions; with a selectivity of 55, 28, and 8%, respectively. This differs from the high selectivity for the acid channel for formic and acetic acids and from the thermodynamic preference for abstraction at the α position, but it is consistent with the experimentally observed preference for the β and the γ positions in larger organic acids. The rate and selectivity are controlled by the strength of hydrogen bonds between the acid group and the hydroxyl radical in the different transition states and do not correlate with the stability of the products. Natural bond orbital analysis was used to quantify the nature and strength of the hydrogen bonds. At 298 K and below 0.1 atm, the collision frequency is insufficient to stabilize the prereactive complexes, and the reaction becomes chemically activated. However, the reaction rate and the selectivity are largely unaffected by this mechanistic change.

1. Introduction

Carboxylic acids are important constituents of the atmosphere and can be found in gaseous phase and in particulate matter, such as fog, clouds, rainwater, snow, and ice.[1] Carboxylic acids together with carbonyl compounds account for a major fraction of the total organic carbon in fog, cloud, and precipitation,[1] and contribute considerably to ambient and precipitation acidity.[2] Carboxylic acids originate from primary anthropogenic sources, such as emissions from wood burning and vehicle exhausts, and from biogenic sources, such as soil and vegetation, as well as from secondary reactions.[1] In addition to dry and wet deposition, atmospheric carboxylic acids can be removed through photochemical oxidation by hydroxyl radicals. The lifetime of carboxylic acids in the atmosphere may vary from several hours to more than one week.[1] The oxidation of organic acids follows a free-radical mechanism in which the initial step is hydrogen abstraction by hydroxyl radicals. This initial step determines the lifetime and, to a large extent, the fate of the oxidation of carboxylic acids.

Experimental studies conclude that hydroxyl radicals preferentially attack the acid hydrogen atom for small carboxylic acids, such as formic and acetic acid.[3−6] For larger carboxylic acids, a change in selectivity is observed. Electron paramagnetic resonance studies indicate that abstraction of a β-hydrogen atom is the dominant mechanism for propionic and butyric acid,[7] while abstraction at both the β- and γ-position was reported for butyric and valeric acid.[8] This change in selectivity has been rationalized by the higher calculated frontier orbital electron density at the β- and γ-positions in larger organic acids.[8]

Theoretical studies of the initial hydrogen abstraction from organic acids by hydroxyl radicals focus mainly on formic[9−11] and acetic acid.[11−13] In agreement with experimental data, abstraction of the acid hydrogen was found to be the dominant mechanism for both acids. Interestingly, the observed dominance of the acid channel at 298 K is caused by the enhancement of the reaction rate for the acid channel by quantum mechanical tunneling and not by a lower activation barrier.[9,11] Our previous study[11] showed that state-of-the-art first principles calculations can begin to predict rate coefficients for reactions between small organic acids and hydroxyl radicals with chemical accuracy (i.e., typically within a factor of 4 of experimental data at 298 K) and that the selectivity between the acid and the C−H channels can be calculated reliably. Quantum mechanical tunneling is, however, very important for the acid channel at temperatures below 400 K, and the small curvature tunneling (SCT) method[14] which accounts for the curvature of the reaction path and approximately incorporates tunneling paths other than the minimum energy path (MEP), is required for accurate results.

In this study, we use first principles calculations to investigate the initial step in the oxidation of carboxylic acids via hydrogen abstraction by hydroxyl radicals, to begin to provide a more detailed understanding of the degradation mechanism of carboxylic acids in the troposphere. Our main objective is to quantify and rationalize the selectivity between the possible pathways. Valeric acid, C_4H_9COOH, was selected as a representative linear carboxylic acid and allows quantifying the selectivity among the acid, α-, β-, γ-, and methyl channel (Scheme 1).

* To whom correspondence should be addressed. Phone: +65 6516 5826. Fax: +65 6779 1936. E-mail: chesm@nus.edu.sg.
[†] Department of Chemical and Biomolecular Engineering.
[‡] Division of Environmental Science and Engineering.

10.1021/jp8090792 CCC: $40.75
Published on Web 06/15/2009

SCHEME 1

Acid channel: $CH_3CH_2CH_2CH_2COOH + OH\bullet \rightarrow CH_3CH_2CH_2CH_2COO\bullet + H_2O$

α-channel: $CH_3CH_2CH_2CH_2COOH + OH\bullet \rightarrow CH_3CH_2CH_2CH\bullet COOH + H_2O$

β-channel: $CH_3CH_2CH_2CH_2COOH + OH\bullet \rightarrow CH_3CH_2CH\bullet CH_2COOH + H_2O$

γ-channel: $CH_3CH_2CH_2CH_2COOH + OH\bullet \rightarrow CH_3CH\bullet CH_2CH_2COOH + H_2O$

Methyl channel: $CH_3CH_2CH_2CH_2COOH + OH\bullet \rightarrow CH_2\bullet CH_2CH_2CH_2COOH + H_2O$

2. Computational Methods

In our previous study of the reaction of formic and acetic acid with hydroxyl radicals,[11] a computational procedure was developed to predict rate coefficients for this family of reactions with chemical accuracy; that is, within a factor 2−4 of experimental data. The procedure is briefly summarized below. Standard enthalpies of formation for the reactants, complexes, transition states, and products are calculated using the complete basis set CBS-QB3 method.[15] This method was found to predict activation barriers and reaction energies for hydrogen abstraction from formic and acetic acid by hydroxyl radicals within 3 kJ/mol[11] and standard enthalpies of formation of hydrocarbons with a mean absolute deviation of 2.5 kJ/mol.[16] Within the CBS-QB3 method, geometries are optimized at the B3LYP/6-311G(d,p) level of theory. For this family of reactions, geometries optimized at the B3LYP/6-311G(d,p) level of theory are essentially similar to geometries optimized using a larger cc-pVTZ basis set and fairly similar to QCISD/6-311++G(d,p) geometries.[11] Intrinsic reaction coordinate calculations[17] were performed to confirm the reaction paths.

In the high-pressure-limit regime, reaction rate coefficients were calculated using the microscopic formulation of transition state theory:

$$k = \boldsymbol{k(T)}\frac{k_B T}{h}\frac{Q_{TS}(T)}{Q_R(T)}e^{\left(\frac{-\Delta E_0(0K)}{RT}\right)} \quad (1)$$

where k_B is the Boltzmann constant, h is the Planck constant, and $Q_R(T)$ and $Q_{TS}(T)$ are the reactant and transition state partition functions, respectively. The activation barrier at 0 K, ΔE_0(0 K), is the energy difference between the transition state and the reactants at 0 K, including the zero point energy (ZPE), and was calculated with the CBS-QB3 method. The tunneling correction factor $\kappa(T)$ accounts for tunneling effects on the reaction rate. Partition functions $Q(T)$ were calculated using standard formulas from statistical thermodynamics.[18] Internal rotation partition functions were obtained using the one-dimensional hindered rotation approximation.[19] Rotational potentials were calculated as a function of the torsion angle at 10° intervals using the B3LYP/6-311G(d,p) method. A 0.9679 scaling factor[20] was used for frequencies that enter the vibrational partition function, and the ZPE was calculated within the CBS-QB3 method. Only the ground state was used to calculate the electronic partition function, except for the hydroxyl radical for which the first excited state, located 1.7 kJ/mol above the ground state,[21] was taken into account. All the first principles calculations were performed with the Gaussian03 computational package.[22]

Tunneling correction factors $\kappa(T)$ were calculated using the small curvature tunneling method, as implemented in the Polyrate9.7[23] and the Gaussrate9.7[24] programs, following the approach outlined earlier.[11] Tunneling calculations are done on the vibrationally adiabatic ground-state potential energy surface and require an accurate description of the energy variation along the reaction path; in particular, near the transition state. Depending on the tunneling approximation, a larger range of the potential energy surface needs to be calculated. Since the CBS-QB3 method was found to provide accurate reaction and activation energies at a reasonable computational cost, geometries along and curvatures orthogonal to the minimum energy path were calculated at the B3LYP/6-311G(d,p) level of theory, whereas the energy variation along the MEP was described using the CBS-QB3 method. This approach is consistent with the approach described by Malick et al.[25] and Saeys et al.[26] and has been implemented using the dual-level VTST-ISPE method in the Polyrate9.7 program.[27] The Page−McIver method[28] was used to follow the reaction coordinate. The reoriented dividing surface algorithm[29] was used to calculate frequencies along the reaction path. In addition, the low real frequency was interpolated with the IVTST0FREQ scheme[23] to avoid imaginary frequencies. For the acid, α1, α2, β, γ, methyl1, and methyl2 channels, the MEPs were mapped with a 0.53 pm step size for reaction coordinates s from −0.69 to +0.98 Å, from −1.19 to +0.29 Å, from −1.24 to +0.24 Å, from −1.52 to +0.24 Å, from −1.52 to +0.29 Å, from −1.19 to +0.24 Å, and from −0.95 to +0.19 Å, respectively, where $s = 0$ indicates the B3LYP/6-311G(d,p) transition state. The Hessians were recalculated every nine steps. CBS-QB3 energies were calculated for the saddle points, for complexes on the reactant and product side, and for additional points at $s = -0.43$, −0.24, −0.11, 0.16, 0.36, and 0.98 Å (acid); $s = -1.19$, −0.71, −0.43, −0.29, −0.14, 0.05, 0.10, 0.14, 0.19, 0.24, and 0.29 Å (α1); $s = -1.24$, −1.14, −0.90, −0.67, −0.43, −0.29, −0.14, 0.05, 0.10, 0.14, 0.19, and 0.24 Å (α2); $s = -1.52$, −0.90, −0.57, −0.14, 0.05, 0.10, 0.14, 0.19, and 0.24 Å (β); $s = -1.52$, −1.29, −0.57, −0.43, −0.29, −0.14, 0.05, 0.10, 0.14, 0.19, 0.24, and 0.29 Å (γ); $s = -1.19$, −0.95, −0.71, −0.43, −0.29, −0.14, 0.05, 0.10, 0.14, 0.19, and 0.24 Å (methyl1); and $s = -0.95$, −0.71, −0.43, −0.29, −0.14, 0.05, 0.10, 0.14, and 0.19 Å (methyl2) along the MEPs. The tunneling correction factors were also calculated with the computationally efficient Eckart method because Eckart tunneling factors were found to agree well with more accurate SCT factors for the C−H channels in formic and acetic acid.[11] The Eckart tunneling factor is obtained by fitting an Eckart potential to the potential energy profile using the B3LYP/6-311G(d,p) curvature at the transition state, and the zero point energy inclusive CBS-QB3 energy barrier and reaction energy. The tunneling factor is then obtained using standard expressions.[30]

Reactions between carboxylic acids and hydroxyl radicals proceed through a hydrogen-bonded prereactive complex.[9−13] First, a chemically activated prereactive complex* is formed, which can undergo stabilization through collisions, where β is the collisional stabilization efficiency, k_s is the collisional stabilization rate coefficient, and [M] is the bath gas concentration; dissociate back to the reactants, k_{-1}; or react to form the products, k_2.

At the high-pressure limit, the prereactive complexes obey a Boltzmann equilibrium population, and the pseudoequilibrium assumption can be used for the formation of the prereactive complexes above 230 K.[11] Indeed, at 298 K, collision theory gives 2×10^7 m^3/(mol s) for k_1, and using calculated equilibrium coefficients of between 6.5×10^{-4} and 1.4×10^{-2} m^3/mol for the formation of the prereactive complexes, k_{-1} is calculated to be between 1.1×10^9 and 2.5×10^{10} s^{-1}. For the reaction between valeric acid and hydroxyl radicals, k_2 is at least 1−2 orders of magnitude smaller than k_{-1} at 298 K, and the pseudoequilibrium assumption is valid. However, consistent with the higher activation barrier, the difference between k_{-1} and k_2

SCHEME 2

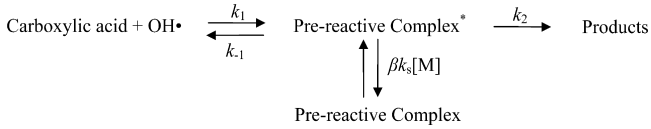

decreases at lower temperatures. Below 230 K, k_{-1} becomes smaller than k_2, and the pseudoequilibrium approximation no longer holds. Using the pseudoequilibrium assumption for the formation of the prereactive complexes, the reaction rate coefficient can be written as[11]

$$k = K_{eq}k_2 = \kappa(T)\frac{k_B T}{h}\frac{Q_{TS}(T)}{Q_R(T)}e^{-(E_{TS}-E_R)/RT} \qquad (2)$$

where $Q_{TS}(T)$ and E_{TS} are the partition function and the energy at 0 K for the transition state, and $Q_R(T)$ and E_R are the partition function and the energy at 0 K for the separated reactants. $\kappa(T)$ is the tunneling correction factor for the hydrogen transfer reaction, step 2 in Scheme 2.

The above calculations are based on transition state theory. At 1 atm and 298 K, the high-pressure-limit assumption may not be valid, and the reaction may be partially chemically activated. Indeed, at low pressures, the collision frequency with bath gas molecules is too low to stabilize the chemically activated prereactive complexes before they undergo further reactions. The effect of pressure on the overall rate coefficients at 298 K was evaluated using the three-frequency version of quantum Rice−Ramsberger−Kassel theory[31] with the modified strong-collision approximation (QRRK−MSC)[32] using CHEMDIS.[33] The MSC approximation assumes that collision either stabilizes the activated complex completely or not at all.[36] Both the chemically activated and thermally activated mechanism are considered in the simulations. Though the effect of the bath gas pressure on the rate coefficient could be treated more accurately using the master equation approach,[34] reasonable agreement between QRRK−MSC estimates and master equation calculations has been reported.[35] The high-pressure-limit rate coefficients $k_1(T)$ and $k_2(T)$ were calculated as above, while $k_{-1}(T)$ was obtained from the equilibrium constant. Within CHEMDIS, the rate coefficients are described by four parameter expressions, $AT^n \exp(-\alpha T) \exp(-E_a/RT)$. Lennard-Jones parameters for the prereactive complexes, $\sigma = 5.85$ Å^2 and $\varepsilon = 327$ K, were taken from literature values for *n*-pentane.[37] N_2 was used as the bath gas. Tunneling corrections are not included in the QRRK−MSC simulations, and the final rate coefficients were obtained by multiplying the pressure-dependent rate coefficients with the corresponding SCT factors, $\kappa_i(298)$.

Hydrogen bonds in the different transition states play an important role in determining the rate and selectivity of the initial hydrogen abstraction from organic acids by hydroxyl radicals. To characterize and quantify the strength of the hydrogen bonds, a natural bond orbital (NBO) analysis was performed at the B3LYP/6-311G(d,p) level of theory using the NBO3.1 package,[38] as implemented in Gaussian03.

3. Results and Discussion

To analyze the selectivity of the initial hydrogen abstraction from organic acids by hydroxyl radicals, hydrogen abstraction at different positions in valeric acid was investigated. First, calculations for the reactant, the different products, and the prereactive hydrogen-bonded complexes are discussed. Next, the stability of the different transition states is calculated, and the strength and nature of the hydrogen bonds is analyzed. Finally, kinetic parameters are derived for the different channels, and the selectivity is discussed.

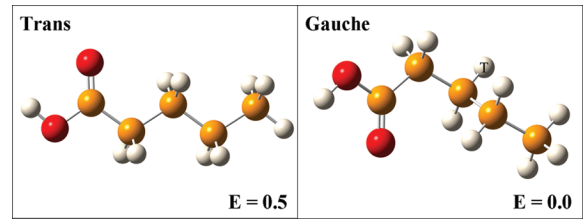

Figure 1. Most stable conformations of valeric acid. CBS-QB3 energies at 0 K (kJ/mol) relative to the gauche conformation are given.

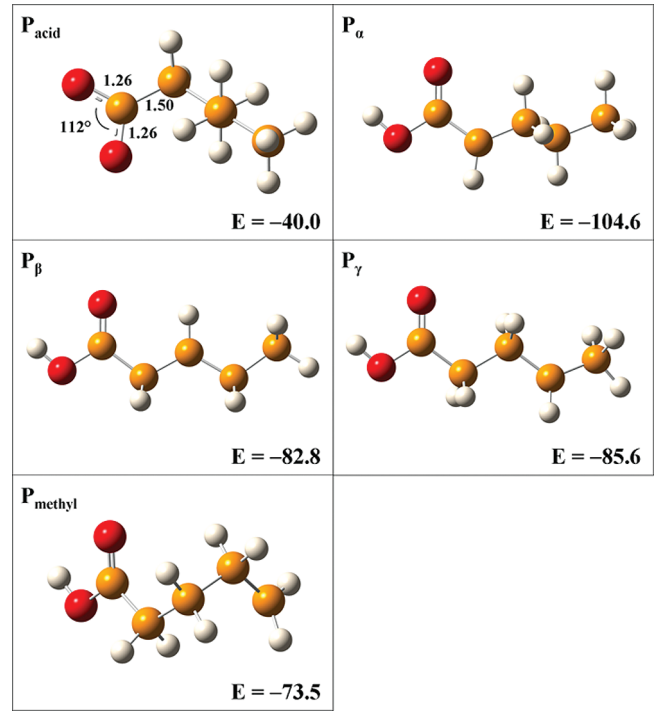

Figure 2. Optimized product structures after hydrogen abstraction from valeric acid and corresponding CBS-QB3 reaction energies at 0 K (kJ/mol). Only the most stable conformations are shown.

Valeric Acid. Various conformations were considered for valeric acid. The two most stable conformations are shown in Figure 1. The all-trans conformation is 0.5 kJ/mol less stable than the conformation with a gauche interaction between the acid and the ethyl group. The stability of the gauche conformation can be attributed to the gauche effect,[39,40] resulting from donation from the C−H σ orbital (trans to the acid group and indicated in Figure 1) to the C−COOH σ^* antibonding orbital. The CBS-QB3 energy at 0 K of the gauche conformation of valeric acid and the hydroxyl radical are the reference energy in this work.

Products. Optimized structures and reaction energies at 0 K for the five radical products in their lowest energy conformation are shown in Figure 2, whereas the corresponding standard enthalpies of formation and the C−H bond dissociation energies (BDEs) are listed in Table 1. The calculated standard enthalpy of formation, $\Delta_f H°$ (298 K), of valeric acid lies within the range of experimental values; that is, between −500.9 and −477.3 kJ/mol.[41] Abstraction of the α-hydrogen is thermodynamically preferred (P_α in Figure 2), with a reaction energy of −104.6 kJ/mol, and is 21.8, 19.0, and 31.1 kJ/mol more favorable than

TABLE 1: Standard Enthalpies of Formation, $\Delta_f H°$ (298 K), and Bond Dissociation Energies, BDE, for the Radicals Formed by Hydrogen Abstraction at Five Positions (indicated in boldface) in Valeric Acid[a]

molecule	Δ_fH° (298 K)[b] (kJ/mol)	BDE at 298 K (kJ/mol)
$CH_3CH_2CH_2CH_2COOH$	−495.1	
$CH_3CH_2CH_2CH_2COO\mathbf{H}$ (acid)	−253.5	461.9
$CH_3CH_2CH_2CH\mathbf{H}COOH$ (α)	−318.0	397.5
$CH_3CH_2CH\mathbf{H}CH_2COOH$ (β)	−294.6	420.9
$CH_3CH\mathbf{H}CH_2CH_2COOH$ (γ)	−297.3	418.1
$CH_2\mathbf{H}CH_2CH_2CH_2COOH$ (methyl)	−286.4	429.1
$CH_3CH\mathbf{H}CH{=}CH_2$ (sec. allylic)	136.8	354.2
$CH_3CH\mathbf{H}CH_2CH_3$ (secondary)	68.8	417.3
$CH_2\mathbf{H}CH_2CH_2CH_3$ (primary)	80.4	428.9

[a] BDEs for butene and butane are provided for comparison. [b] calculated following the procedures in ref. 26.

abstraction of a β-, γ-, or methyl hydrogen, respectively, and 64.6 kJ/mol more favorable than abstraction of the acid hydrogen (Figure 2). Abstraction at the α-position in valeric acid is also 20.3 kJ/mol more exothermic than the corresponding methyl channel in acetic acid,[11] consistent with the higher stability of a secondary radical. The relative stability of P_α can be attributed to resonance with the C═O bond. The stabilization is less than with a C═C double bond, and the BDE for a secondary allylic C−H bond, 351.9 kJ/mol, is lower than for the α C−H bond in valeric acid, 397.5 kJ/mol (Table 1).

Abstraction of the acid hydrogen is thermodynamically the least favorable; however, this reaction is kinetically preferred for formic and acetic acid. Various nearly degenerate, low-lying electronic states have been identified for acyloxyl radicals.[11,42,43] For the smallest acyloxyl radical, HCOO•, the $^2B_2$ state is about 8 kJ/mol more stable than the $^2A_1$ state and about 10 kJ/mol more stable than the $^2A'$ state.[43] Three related states could also be optimized for the corresponding pentanoyloxidanyl radical (P_{acid}); the most stable state is shown in Figure 2. This state is electronically and structurally similar to the $^2B_2$ state for HCOO•. The calculated reaction energy of −40.0 kJ/mol is similar to the value for acetic acid, −40.8 kJ/mol.[11]

The reaction energies and BDEs for the β- and γ-channels are typical for secondary carbon atoms and can be compared to the values for *n*-butane (Table 1). Abstraction of a methyl hydrogen atom is the least favorable C−H channel, and the corresponding BDE is typical for a primary carbon atom. On the basis of thermodynamic arguments, abstraction of the α-hydrogen would be expected to be the dominant reaction.

Prereactive Complexes. The formation of prereactive complexes is common in reactions involving hydroxyl radicals.[9−13] Three prereactive complexes can be identified for the reaction between valeric acid and a hydroxyl radical (Figure 3), and the structure and the stability of the complexes are similar to acetic acid.[11]

Prereactive complexes are important to understand the kinetics of hydrogen abstraction from carboxylic acids. The presence of prereactive complexes allows the transition states to be lower in energy than the separated reactants, valeric acid, and a hydroxyl radical, leading to negative overall activation energies (eq 2). In the low temperature mechanism, a hydroxyl radical is first captured by the acid group before abstracting a hydrogen atom. As discussed in the next section, the interaction between the hydroxyl radical and the acid group determines which hydrogen along the alkyl chain will be abstracted. Hydrogen bond complexes between the product radicals and water can also be identified. Details on product complexes for this family of reactions have been reported previously.[11]

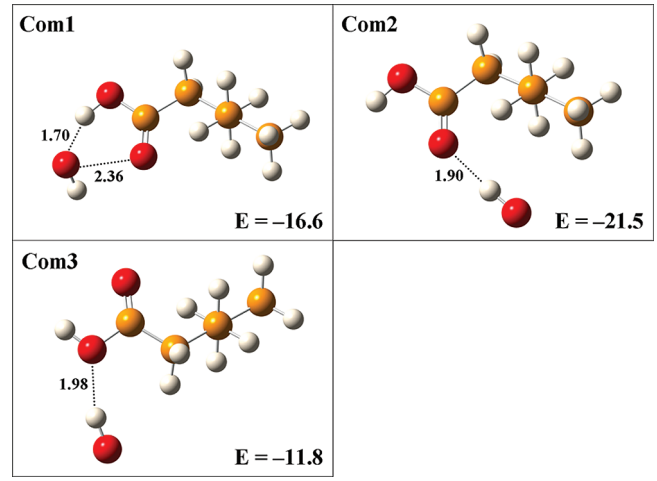

Figure 3. Prereactive complexes between valeric acid and a hydroxyl radical. Selected bond lengths (Å) and CBS-QB3 energies at 0 K (kJ/mol, relative to the reactants) are indicated.

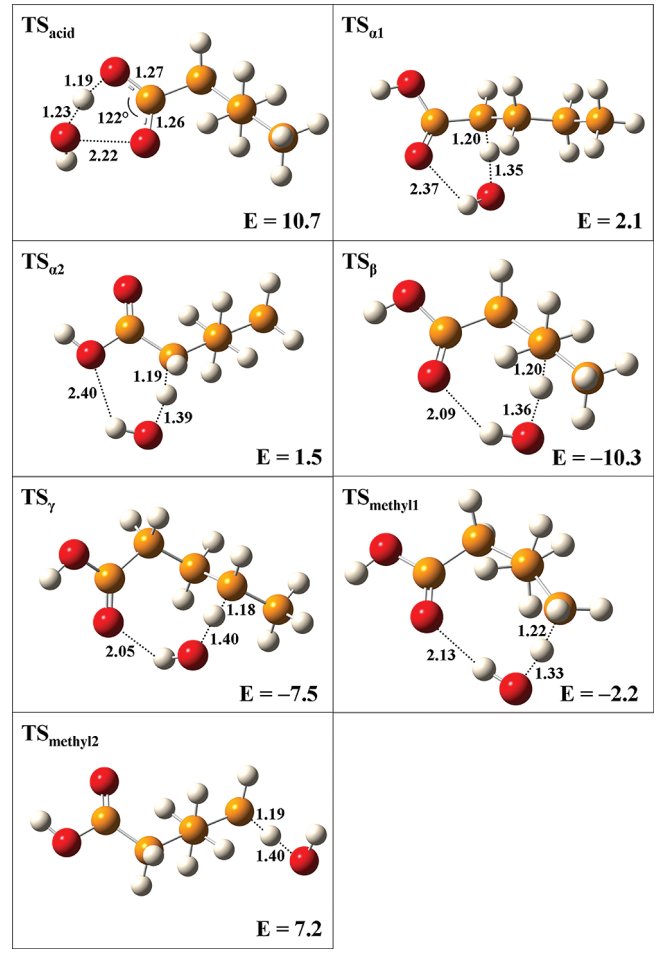

Figure 4. Optimized transition state structures for the reaction between valeric acid and a hydroxyl radical. Selected bond lengths (Å) and CBS-QB3 energies at 0 K (kJ/mol, relative to the separate reactants) are indicated.

Transition States. Optimized transition state structures and energies relative to the separated reactants are shown in Figure 4. The hydrogen bonds between the hydroxyl radical and the acid group in the prereactive complexes are still present in the transition states for the α, β, γ, and methyl channels, and

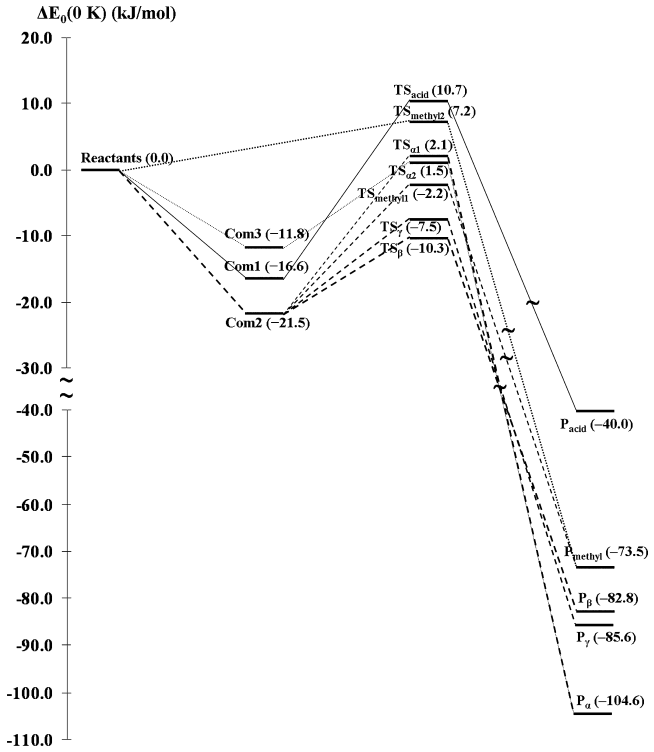

Figure 5. Potential energy profiles for the reaction between valeric acid and a hydroxyl radical. CBS-QB3 energies at 0 K relative to the separated reactants are indicated. Product complexes are omitted to simplify the diagram.

the transition state structures are characterized by six-, seven-, eight-, and nine-member rings, respectively. The O···HO bond lengths range from 2.05 to 2.40 Å and are longer than the O···HO• bond length in the prereactive complexes; that is, 1.90 (Com2) and 1.98 Å (Com3). This may indicate that the hydrogen bonds in the transition states are somewhat weaker than the 21.5 kJ/mol calculated for the prereactive complex, Com2. For an optimal overlap between the donating oxygen lone pair and the accepting σ^* hydroxyl orbital, the acid group and the hydroxyl radical need to be nearly coplanar. This is, indeed, observed for Com2, with an O−C═O···H dihedral angle of 1°. However, the ring structures in the transition states do not always allow an optimal overlap, and the O−C═O···H dihedral angles are 22°, 66°, and 3° for the β (TS_β), γ (TS_γ), and methyl ($TS_{methyl1}$) channels, respectively.

The transition state structure for the acid channel (TS_{acid}) is similar to the transition state structure for the reaction between acetic acid and a hydroxyl radical, and the activation barrier of 10.7 kJ/mol is also similar to the 11.0 kJ/mol barrier calculated for acetic acid.[11] Following the reaction path toward the reactants leads to the prereactive complex Com1 (Figure 5). Two low energy transition states could be optimized for the α channel ($TS_{\alpha1}$ and $TS_{\alpha2}$). Both structures can again be compared with the acetic acid reaction, although the transition states for valeric acid are somewhat earlier. Indeed, the breaking C−H bonds are 0.04 Å shorter and the forming H−O bonds are 0.07 Å longer than for the acetic acid reaction. This is consistent with the higher stability of the products for valeric acid. The barriers, 2.1 and 1.5 kJ/mol for $TS_{\alpha1}$ and $TS_{\alpha2}$, respectively, are 9.8 and 11.0 kJ/mol lower than the corresponding barriers for acetic acid, again consistent with the higher exothermicity for the reaction with valeric acid. Following the reaction path from $TS_{\alpha1}$ leads to prereactive complex Com2, whereas starting from $TS_{\alpha2}$ leads to Com3 (Figure 5). The barriers for the α channel are significantly lower than the barriers for the acid channel, and the acid channel can be expected to be less important for larger organic acids.

TABLE 2: High-Pressure-Limit Reaction Rate Coefficients; Reaction Barriers, ΔE_0(0 K); Selectivity, SCT, and Eckart Tunneling Correction Factors; and Activation Entropies, $\Delta S^\circ\ddagger$, at 298 K for the Different Reaction Channels

channel	rate coefficient 10^5 m^3/(mol s)	ΔE_0 (0 K) kJ/mol	selectivity; %	tunneling factor	$\Delta S^\circ\ddagger$[a] J/(K mol)
acid	3.38	10.7	8	113 (6.3[b])	−130
α1	0.872	2.1	2	1.9 (2.0[b])	−134
α2	1.75	1.5	4	1.3 (1.3[b])	−128
β	23.5	−10.3	55	1.3 (1.5[b])	−151
γ	12.1	−7.5	28	1.2 (1.2[b])	−149
methyl1	0.454	−2.2	1	1.9 (2.6[b])	−167
methyl2	1.07	7.2	2	1.2 (1.2[b])	−100
overall	43.1				

[a] $\Delta S^\circ\ddagger$ is the difference between the entropy of the transition state and the separated reactants at 298 K. [b] Eckart tunneling correction factors in parentheses.

The transition state for the β-channel, TS_β, is the most favorable among the channels considered, and lies 10.3 kJ/mol below the energy level of the reactants. Note that this is possible because of the stability of the corresponding prereactive complex, Com2. The activation barrier for the β-channel is 11.8 kJ/mol lower than the barrier for the α channel, despite the lower stability of the product for the β channel. Clearly, the activation barriers for hydrogen abstraction from organic acids by hydroxyl radicals are not determined by the reaction energy and do not follow an Evans−Polanyi-type correlation.[44] Instead, as discussed below, the activation barriers are determined mainly by the strength of the hydrogen bond present in the transition state. The lengths of the breaking and forming bonds in TS_β are similar to TS_α; however, the C═O···HO hydrogen bond is significantly shorter. A transition state structure analogous to $TS_{\alpha2}$ was found to be 8.2 kJ/mol less stable than TS_β, and is therefore not included in Figure 4.

The transition state for the γ-channel, TS_γ, is 2.8 kJ/mol less stable than the transition state for the β-channel, but it still lies 7.5 kJ/mol below the energy level of the separated reactants. The lower stability of TS_γ is likely caused by a weaker hydrogen bond resulting from a less optimal overlap between the σ^* hydroxyl orbital and an oxygen lone pair, as indicated by the O−C═O···H dihedral angle of 66°. This will be further quantified by the NBO analysis below. The transition state structure for the γ-channel is characterized by an eight-member ring (Figure 4). Also for abstraction of the methyl hydrogen atom, a hydrogen bond is found in the transition state structure, $TS_{methyl1}$. The 8.1 kJ/mol higher activation barrier for $TS_{methyl1}$ compared to TS_β can be attributed mainly to the stronger methyl C−H bond (Table 1). A NBO analysis indicates that the hydrogen bond in $TS_{methyl1}$ is only slightly weaker than in TS_β, consistent with the comparable dihedral angles and C═O···HO distances.

The reaction rate coefficient is determined not only by the activation barrier, but also by the entropy cost to reach the transition state. The activation entropies for the different channels are given in Table 2. The formation of a ring converts degrees of freedom for the rotation around the C−C bonds to low-frequency ring vibrations. This lowers the entropy of the transition state. Calculations indicate that the entropy contribution for an internal rotor is about 20 J/(mol K) at 298 K. Indeed, the activation entropy, $\Delta S^\circ\ddagger$, decreases every time the ring increases by one CH_2 group, and hence, the preexponential

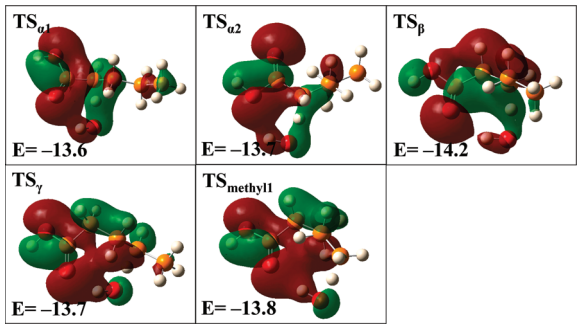

Figure 6. Molecular orbitals involved in the hydrogen bond between the hydroxyl radical and the oxygen lone pairs for the different transition states. Orbitals were calculated at the B3LYP/6-311G(d,p) level, and isosurfaces for electron densities of 0.02 e/Å^3 are shown. The B3LYP energy levels (eV) of the molecular orbitals are indicated.

SCHEME 3

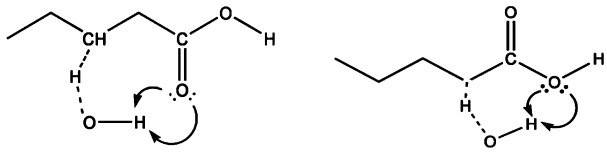

factor decreases. As a consequence, for a certain ring size, the entropy cost of forming a ring outweighs the energy gained by forming a hydrogen bond. The entropy for TS$_\gamma$ deviates from the trend, again because of the weaker hydrogen bond. Indeed, the vibration frequency corresponding to the pseudorotation of the ethyl group in the eight-member ring of TS$_\gamma$ is very low, leading to a smaller entropy loss. To consider the competition between enthalpy gain and entropy cost, the transition state for the methyl channel without a hydrogen bond was optimized, TS$_{methyl2}$. Although TS$_{methyl2}$ is 9.4 kJ/mol less stable than TS$_{methyl1}$, the entropy difference of 67 J/(mol K) at 298 K more than compensates for this, resulting in a 40% higher reaction rate coefficient than for the reaction via the energetically more favorable TS$_{methyl1}$ (Table 2). For the β and γ channels, the smaller entropy cost is not able to compensate for the higher activation barrier, and a mechanism via a transition state without a hydrogen bond is at least 100 times slower at 298 K.

Selected molecular orbitals involved in the hydrogen bond between the hydroxyl radical and the acid group are shown in Figure 6. The electron density contour plots illustrate the interaction between the oxygen lone pairs and the σ^* orbital of the hydroxyl radical, as indicated in Scheme 3.

To quantify the relative strengths of the hydrogen bonds and to evaluate the electron transfer from the oxygen lone pairs to the σ^*_{OH} orbital, a NBO analysis was performed. Electron occupancies for the involved NBOs and the resulting charge transfer delocalization energies are summarized in Table 3 for the transition states and for the prereactive complexes, Com2 and Com3. According to a NBO analysis, hydrogen bonds result from electron donation from an oxygen lone pair (n_O, Lewis base) to the antibonding σ^*_{OH} orbital of the hydroxyl radical (Lewis acid).[45] The strength of the interaction can be quantified by the charge transfer delocalization energy (ΔE_{CT}).[45] The NBO analysis indicates that the strongest hydrogen bonds are found for the prereactive complexes, followed by TS$_\beta$ and TS$_{methyl1}$. This is generally consistent with the O−C═O···H dihedral angles and O···HO bond lengths reported earlier. The ΔE_{CT}'s for the prereactive complexes, 35.1 and 21.9 kJ/mol, are significantly larger than for the transition states. For the α channel, electron transfer and ΔE_{CT} are more pronounced for

TABLE 3: Natural Bond Orbital Analysis of the Occupancy of the Oxygen Lone Pairs on the Acid Group, n_{1O}, and n_{2O}, and of the Antibonding σ^*_{OH} Orbital in the Hydroxyl Radical, and Resulting Charge Transfer Delocalization Energies, ΔE_{CT} (kJ/mol), for the Prereactive Complexes and the Transition States

	Com2	Com3	TS$_{\alpha1}$	TS$_{\alpha2}$	TS$_\beta$	TS$_\gamma$	TS$_{methyl1}$
			Occupancy				
n_{1O}[a]	1.968	(1.970)	1.977	(1.978)	1.974	1.974	1.973
n_{2O}[a]	1.855	(1.844)	1.849	(1.832)	1.850	1.853	1.853
σ^*_{OH}	0.019	0.014	0.006	0.003	0.011	0.010	0.009
			ΔE_{CT}				
$n_{1O} \rightarrow \sigma^*_{OH}$	16.8	18.8	0.1	1.1	4.1	4.8	5.7
$n_{2O} \rightarrow \sigma^*_{OH}$	18.3	3.1	3.4	1.1	10.3	2.6	8.4
total	35.1	21.9	3.5	2.2	14.4	7.4	14.1

[a] NBO occupancies for the −C(**O**)OH and −C(**O**)OH (parentheses) lone pairs (Scheme 3).

TABLE 4: Small Curvature Tunneling Correction Factors for the Different Reaction Channels (Figure 5)

T (K)	acid	α1	α2	β	γ	methyl1	methyl2
200	5343	4.2	2.0	1.9	1.5	4.4	1.7
400	19.2	1.4	1.2	1.2	1.1	1.4	1.1
500	7.6	1.2	1.1	1.1	1.1	1.3	1.1
600	4.4	1.2	1.1	1.1	1.1	1.2	1.1

the TS$_{\alpha1}$ transition state than for the TS$_{\alpha2}$ transition state and significantly smaller than for the other transition states and for the prereactive complexes. This is consistent with the higher activation barriers for the α-channel. The ΔE_{CT} and the electron transfer are largest for TS$_\beta$ and TS$_{methyl1}$, indicating strong hydrogen bonds. Although the occupancies for TS$_\gamma$, TS$_\beta$, and TS$_{methyl1}$ are similar, the charge transfer delocalization energy is 7.0 kJ/mol smaller for TS$_\gamma$ than for TS$_\beta$. This is caused by the unfavorable overlap between the oxygen lone pair and the σ^*_{OH} orbital in TS$_\gamma$, reflected by the O−C═O···H dihedral angle of 66°. Indeed, a hydrogen bond is strongest for near-linear alignment of n_O and σ^*_{OH} to achieve maximum orbital overlap.[44] The hydrogen bond in TS$_{methyl1}$ is nearly as strong as in TS$_\beta$.

In summary, hydrogen bonds are found to significantly stabilize the transition states for hydrogen abstraction from organic acids by hydroxyl radicals, and competition between stabilizing hydrogen bonds and the entropy cost to form a ring structure determines the selectivity between the different channels. It should be noted that the reported calculations were performed for gas-phase reactions. From the results, it can be expected that the presence of water molecules might have an important effect on the formation of hydrogen bonds, and an important change in the selectivity and possibly in the reaction rate coefficients might be envisioned in the presence of water. Such studies are, however, beyond the scope of this work. To further quantify the selectivity between the different reaction pathways, tunneling correction factors and reaction rate coefficients are reported in the next section.

Kinetic Parameters and Reaction Path Analysis. Calculated reaction rate coefficients, tunneling correction factors, selectivities, and activation entropies at 298 K and for the high-pressure-limit regime are presented in Table 2 for the various reaction channels. SCT correction factors between 200 and 600 K for all the channels are shown in Table 4. The overall reaction rate coefficient of 43.1×10^5 m^3/(mol s) for the reaction between valeric acid and hydroxyl radicals at 298 K is significantly higher than the calculated rate coefficients for formic acid, 0.98×10^5 m^3/(mol s), and for acetic acid, 1.2×10^5 m^3/(mol s)[11]. The

rate coefficient for the acid channel, 3.4×10^5 m^3/(mol s), can be compared with the corresponding experimental rate coefficients for the acid channel in formic acid, 2.0×10^5 m^3/(mol s),[4] and in acetic acid, $(2.5 \pm 0.7) \times 10^5$ m^3/(mol s),[6] and is a factor of 3−4 higher than the corresponding theoretical rate coefficients for acetic acid, 1.2×10^5 m^3/(mol s), and formic acid, 0.85×10^5 m^3/(mol s).[11] However, the selectivity for the acid channel is only 8%, much lower than the selectivity of more than 90% for formic and acetic acid. Tunneling significantly enhances the rate for the acid channel at 298 K, and the small curvature tunneling method, which accounts for the curvature of the reaction path and approximately incorporates tunneling paths other than along the minimum energy path, is required to describe the effect of tunneling for the acid channel. The tunneling correction factor at 298 K, 113, is lower than the values for formic acid, 339, and for acetic acid, 199, and the higher rate coefficient for the acid channel in valeric acid can be attributed mainly to the activation entropy of only −130 J/(mol K), as compared to −138 J/(mol K) for the acetic acid reaction.[11] Interestingly, the smaller entropy loss can be attributed to an increase in the hindered rotor entropy for the $C_\alpha-C_\beta$ bond, which is caused by reduction of the gauche effect in the transition state. For the α, β, γ, and methyl C−H channels, the Eckart tunneling correction factors agree well with the more expensive SCT correction factors. The largest deviation at 298 K is 37% for the methyl1 channel, and the agreement improves at higher temperatures. For the acid channel, however, the SCT factor is 53 times larger than the Eckart tunneling factor at 200 K. The high tunneling correction factor for the acid channel can be attributed to the strong reaction path curvature coupling.[11] This effect is much smaller for the C−H channels.

The rate coefficient for the thermodynamically preferred α-channel, 2.6×10^5 m^3/(mol s), is slightly lower than the rate coefficient for the acid channel, despite the lower activation barrier. This can be attributed to the high tunneling correction for the acid channel. The dominant reaction path is found to be abstraction of a β-hydrogen atom, with a calculated rate coefficient of 23.5×10^5 m^3/(mol s). At 298 K, the selectivity for this channel is 55%. The rate coefficient for the γ-channel is about half the value for the β-channel. The lower rate coefficient for the γ-channel is caused by the higher activation barrier, not by the entropy cost to form a larger ring. Two mechanisms were considered for the methyl channel. Both are significantly slower than the β-channel at 298 K. Interestingly, the mechanism via a transition state with a hydrogen bond, $TS_{methyl1}$, is slower than the mechanism through a transition state without a hydrogen bond, $TS_{methyl2}$. In this case, the entropy cost outweighs the energy gain. The rate coefficient for the latter mechanism, 1.07×10^5 m^3/(mol s), is similar to the experimental rate coefficient for hydrogen abstraction from ethane by a hydroxyl radical, 1.48×10^5 m^3/(mol s).[46]

An Arrhenius plot of the rate coefficients for the five channels in the high-pressure-limit regime is shown in Figure 7. Because of the negative overall activation barrier, the rate coefficient for the β- and γ-channel decreases with temperature. Since the barrier for the β channel is the lowest, it becomes more dominant at lower temperature. The rate coefficient for the α-channel, that is, the sum for the α_1 and the α_2 channels, is nearly independent of temperature. The rate coefficient for the acid channel also decreases with temperature. For the acid channel, this is caused not by a negative overall activation barrier, but by the rapid decrease of the tunneling correction factor with temperature (Table 4).[11] At temperatures above about 700 K, the rate for the acid channel increases with temperature,

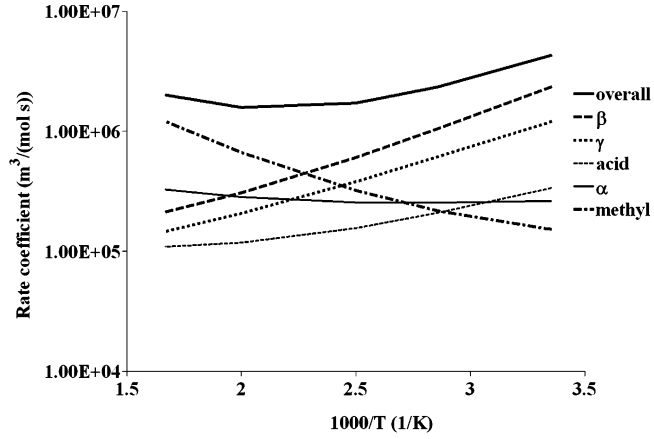

Figure 7. Arrhenius plot of the rate coefficients for the five channels for hydrogen abstraction from valeric acid by hydroxyl radicals between 298 and 600 K in the high-pressure-limit regime.

SCHEME 4

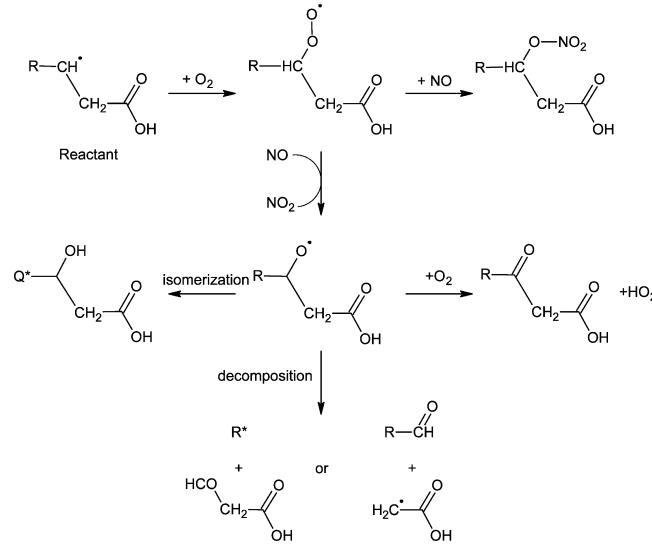

consistent with an activation barrier of 10.7 kJ/mol. The rate coefficient of the methyl channel decreases with temperature below 270 K, but increases with temperature above 270 K. Below 270 K, the mechanism via the transition state with a hydrogen bond, $TS_{methyl1}$, is dominant. The overall activation barrier for this channel is slightly negative at −2.2 kJ/mol. Above 270 K, the mechanism through a transition state without hydrogen bond, $TS_{methyl2}$, is more important, corresponding with a positive activation barrier of +7.2 kJ/mol.

The dominance of the β- and γ-channel, hence follows from the stabilizing hydrogen bond interactions in the transition state and from the entropy cost to form large ring structures. Both effects are well-established, even if the accuracy of state-of-the-art calculations does not allow determining the exact selectivity within a few percent. The preference for the β- and γ-channels has also been observed experimentally for propionic, butyric acid, and valeric acids.[7,8] The abstraction of a hydrogen atom is the initial step in the oxidation mechanism. The next steps are briefly summarized in Scheme 4. The formation of an alkyl radical is generally followed by the addition of O_2 to form a peroxy radical.[47] The peroxy radicals then react with NO to form alkoxy radicals, which can undergo different reactions, such as oxidation, isomerization, and decomposition. On the basis of the high selectivity of the β channel, RC(═O)-CH_2COOH, $CH(═O)CH_2COOH$, RCHO, and $•CH_2COOH$

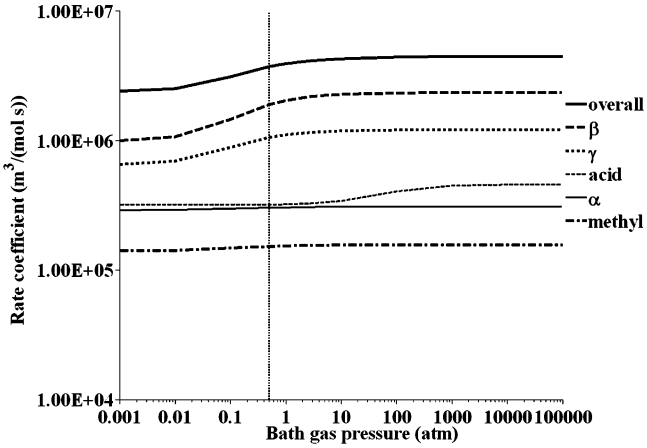

Figure 8. Effect of the N_2 bath gas pressure on the rate coefficients for the five reaction channels at 298 K. The pressure for which the stabilization rate, $\beta k_s[N_2]$ in Scheme 2, becomes equal to reaction rate through the chemically activated complex Com2*, $k_2 + k_{-1}$ in Scheme 2, is indicated.

would be expected as the primary products of the oxidation of long-chain organic acids.

Effect of the Bath Gas Pressure on the Reaction Rate Coefficients and the Selectivity. To evaluate the effect of the bath gas pressure on the rate and selectivity of hydrogen abstraction from organic acids by hydroxyl radicals, we performed QRRK−MSC simulations using N_2 as the bath gas. The results are summarized in Figure 8. Valeric acid reacts with hydroxyl radicals to form chemically activated complexes, Com1*, Com2*, and Com3*. The activated complexes can dissociate back to reactants, form stabilized complexes by collision with bath gas molecules, or undergo hydrogen abstraction to form products, as indicated in Scheme 2. At 1 atm and 298 K, a collisional stabilization rate, $\beta k_s[N_2]$ in Scheme 2, of 5.03×10^9 s^{-1} is calculated for Com2* using QRRK−MSC. At these conditions, the rate coefficient for direct decomposition of the chemically activated complex Com2* via the α1, β, γ, and Me1 channels, k_2 in Scheme 2, is 1.02×10^9 s^{-1}. Direct decomposition is, hence, 5 times slower than collisional stabilization at 298 K and 1 atm. The stabilized complexes can be reactivated by collisions and dissociate to reactants or products via a thermally activated mechanism. Figure 8 shows the overall rate coefficient from reactants to products through both the chemically activated and the thermally activated mechanism as a function of the bath gas pressure. Below about 0.1 atm, the path via the chemically activated complexes dominates. Above 1.0 atm, the collision frequency becomes competitive with the chemically activated hydrogen abstraction mechanism, and stabilized prereactive complexes are formed before converting to products. Although the rate coefficients for direct hydrogen abstraction via the chemically activated complexes decrease with pressure, hydrogen abstraction via the stabilized prereactive complexes becomes more important. As a consequence, the overall rate coefficient (i.e., the sum of the chemically activated and the thermally activated path) increases by less than a factor of 2 from the low-pressure to the high-pressure limit. Moreover, the selectivity remains essentially unchanged; the selectivity for the dominant β-channel increases from 52 to 55% from the low-pressure to the high-pressure limits. The lower overall rate coefficient at low bath gas pressures can be rationalized by the rapid increase of k_{-1} at lower pressures. Indeed, the average internal energy of the prereactive complexes increases when the bath gas pressure decreases, and this leads to an increase in both the H-abstraction rate coefficients, k_2, and the decomposition rate coefficient, k_{-1}. The effect on k_{-1} is, however, larger than the effect on k_2, and for Com2*, the k_{-1}/k_2 ratio increases from 4.9 at the high-pressure limit to 10.3 at the low-pressure limit. A similar change is calculated for the other prereactive complexes.

At 298 K and 1 atm, hydrogen abstraction from valeric acid by hydroxyl radicals is dominantly thermally activated and close to the high-pressure-limit regime. However, the rate coefficient and selectivity are relatively unaffected by the bath gas pressure. Indeed, also in the low-pressure limit, the selectivity between hydrogen abstraction channels starting from the same prereactive complex is proportional to the density of states of the corresponding transition states and is, hence, determined by the relative heights of the activation barriers.[34] Therefore, the selectivity in the low pressure limit is similar to the selectivity in the high pressure limit. Conceptually, however, the reaction proceeds via a different mechanism at low pressures, and stable prereactive complexes are no longer formed.

4. Conclusion

CBS-QB3 quantum chemical calculations were performed to help elucidate the selectivity of the initial hydrogen abstraction from organic acids by hydroxyl radicals. This reaction is the first step in the photochemical oxidation of carboxylic acids in the troposphere and determines their fate. Valeric acid was selected as a representative linear carboxylic acid, and five possible mechanisms were considered: abstraction of the acid and the α, β, γ, and methyl (δ) hydrogen.

Abstraction of the β- and γ-hydrogen atoms dominates with a selectivity of 55% and 28%, respectively, at 298 K. The reaction rate and selectivity are only a weak function of the bath gas pressure. Below 0.1 atm, the reaction becomes chemically activated, but abstraction of the β- and γ-hydrogen atoms remains dominant. This selectivity differs from the high preference for the acid hydrogen observed for smaller carboxylic acids at ambient conditions. The dominance of the β- and γ-channels can be attributed to the presence of a hydrogen bond between the acid group and the attacking hydroxyl radical. This hydrogen bond stabilizes the transition state and leads to ring structures. The reaction between a hydroxyl radical and a carboxylic acid begins with the formation of a hydrogen-bonded prereactive complex. The hydrogen bond is still present in the transition state and determines the selectivity of the reaction. Abstraction of a α hydrogen atom is difficult because its proximity to the acid group does not allow the formation of a stable ring structure. The transition states for abstraction of the β- and γ-hydrogen atoms are characterized by favorable 7- and 8-member rings. Abstraction of hydrogen atoms farther from the acid group requires the formation of larger rings and is, hence, associated with a high entropy cost. Indeed, two mechanisms were considered for abstraction of the δ hydrogen atoms. At 298 K, the rate coefficient for the mechanism via a transition state without a hydrogen bond is 36% faster than the mechanism via a transition state with a hydrogen bond.

Acknowledgment. This work was financially supported by the National University of Singapore. We thank an anonymous referee for valuable suggestions.

Supporting Information Available: Cartesian coordinates and energies (hartree) at 0 K, including zero-point energy calculated using the CBS-QB3 method for reactants, products, prereactive complexes, and transition states. This material is available free of charge via the Internet at http://pubs.acs.org.

References and Notes

(1) Chebbi, A.; Carlier, P. *Atmos. Environ.* **1996**, *30*, 4233–4249.

(2) Dabek-Zlotorzynska, E.; McGrath, M. *Fresenius' J. Anal. Chem.* **2000**, *367*, 507–518.

(3) Wine, P. H.; Astalos, R. J.; Mauldin, R. L., III *J. Phys. Chem.* **1985**, *89*, 2620–2624.

(4) Singleton, D. L.; Paraskevopoulos, G.; Irwin, R. S.; Jolly, G. S.; McKenney, D. J. *J. Am. Chem. Soc.* **1988**, *110*, 7786–7790.

(5) Singleton, D. L.; Paraskevopoulos, G.; Irwin, R. S. *J. Am. Chem. Soc.* **1989**, *111*, 5248–5251.

(6) Butkovskaya, N. I.; Kukui, A.; Pouvesle, N.; Le Bras, G. *J. Phys. Chem. A* **2004**, *108*, 7021–7026.

(7) Taniguchi, H.; Fukui, K.; Ohnishi, S.; Hatano, H.; Hasegawa, H.; Maruyama, T. *J. Phys. Chem.* **1968**, *72*, 1926–1931.

(8) Serpone, N.; Martin, J.; Horikoshi, S.; Hidaka, H. *J. Photochem. Photobiol., A* **2005**, *169*, 235–251.

(9) Galano, A.; Alvarez-Idaboy, J. R.; Ruiz-Santoyo, M. E.; Vivier-Bunge, A. *J. Phys. Chem. A* **2002**, *106*, 9520–9528.

(10) Anglada, J. M. *J. Am. Chem. Soc.* **2004**, *126*, 9809–9820.

(11) Sun, W.; Saeys, M. *J. Phys. Chem. A* **2008**, *112*, 6918–6928.

(12) De Smedt, F.; Bui, X. V.; Nguyen, T. L.; Peeters, J.; Vereecken, L. *J. Phys. Chem. A* **2005**, *109*, 2401–2409.

(13) Rosado-Reyes, C. M.; Francisco, J. S. *J. Phys. Chem. A* **2006**, *110*, 4419–4433.

(14) Skodje, R. T.; Truhlar, D. G.; Garrett, B. C. *J. Phys. Chem.* **1981**, *85*, 3019–3023.

(15) Montgomery, J. A., Jr.; Frisch, M. J.; Ochterski, J. W.; Petersson, G. A. *J. Chem. Phys.* **1999**, *110*, 2822–2827.

(16) Saeys, M.; Reyniers, M. F.; Van Speybroeck, V.; Waroquier, M.; Marin, G. B. *ChemPhysChem* **2006**, *7*, 188–199.

(17) Gonzalez, C.; Schlegel, H. B. *J. Chem. Phys.* **1989**, *90*, 2154–2161.

(18) Mcquarrie, D. A. *Statistical Mechanics*; University Science Books: Sausalito, CA, 2000.

(19) Sumathi, R.; Carstensen, H. H.; Green, W. H., Jr. *J. Phys. Chem. A* **2001**, *105*, 6910–6925.

(20) Andersson, M. P.; Uvdal, P. *J. Phys. Chem. A* **2005**, *109*, 2937–2941.

(21) Chase, M. W. *J. Phys. Chem. Ref. Data*, 1998; monograph 9.

(22) Frisch, M. J.; Trucks, G. W.; Schlegel, H. B.; Scuseria, G. E.; Robb, M. A.; Cheeseman, J. R.; Montgomery, J. A., Jr.; Vreven, T.; Kudin, K. N.; Burant, J. C.; Millam, J. M.; Iyengar, S. S.; Tomasi, J.; Barone, V.; Mennucci, B.; Cossi, M.; Scalmani, G.; Rega, N.; Petersson, G. A.; Nakatsuji, H.; Hada, M.; Ehara, M.; Toyota, K.; Fukuda, R.; Hasegawa, J.; Ishida, M.; Nakajima, T.; Honda, Y.; Kitao, O.; Nakai, H.; Klene, M.; Li, X.; Knox, J. E.; Hratchian, H. P.; Cross, J. B.; Bakken, V.; Adamo, C.; Jaramillo, J.; Gomperts, R.; Stratmann, R. E.; Yazyev, O.; Austin, A. J.; Cammi, R.; Pomelli, C.; Ochterski, J. W.; Ayala, P. Y.; Morokuma, K.; Voth, G. A.; Salvador, P.; Dannenberg, J. J.; Zakrzewski, V. G.; Dapprich, S.; Daniels, A. D.; Strain, M. C.; Farkas, O.; Malick, D. K.; Rabuck, A. D.; Raghavachari, K.; Foresman, J. B.; Ortiz, J. V.; Cui, Q.; Baboul, A. G.; Clifford, S.; Cioslowski, J.; Stefanov, B. B.; Liu, G.; Liashenko, A.; Piskorz, P.; Komaromi, I.; Martin, R. L.; Fox, D. J.; Keith, T.; Al-Laham, M. A.; Peng, C. Y.; Nanayakkara, A.; Challacombe, M.; Gill, P. M. W.; Johnson, B.; Chen, W.; Wong, M. W.; Gonzalez, C.; Pople, J. A. *Gaussian 03, Revision C.02*; Gaussian, Inc.: Wallingford, CT, 2004.

(23) Corchado, J. C.; Chuang, Y. Y.; Fast, P. L.; Hu, W. P.; Liu, Y. P.; Lynch, G. C.; Nguyen, K. A.; Jackels, C. F.; Ramos, A. F.; Ellingson, B. A.; Lynch, B. J.; Melissas, V. S.; Villà, J.; Rossi, I.; Coitiño, E. L.; Pu, J.; Albu, T. V.; Steckler, R.; Garrett, B. C.; Isaacson, A. D.; Truhlar, D. G. *POLYRATE, version 9.7*; University of Minnesota: Minneapolis, MN, 2007.

(24) Corchado, J. C.; Chuang, Y. Y.; Coitiño, E. L.; Truhlar, D. G. *GAUSSRATE, version 9.7*; University of Minnesota: Minneapolis, MN, 2007.

(25) Malick, D. K.; Petersson, G. A.; Montgomery, J. A., Jr. *J. Chem. Phys.* **1998**, *108*, 5704–5713.

(26) Saeys, M.; Reyniers, M. F.; Marin, G. B.; Van Speybroeck, V.; Waroquier, M. *J. Phys. Chem. A* **2003**, *107*, 9147–9159.

(27) Chuang, Y. Y.; Corchado, J. C.; Truhlar, D. G. *J. Phys. Chem. A* **1999**, *103*, 1140–1149.

(28) Page, M.; McIver, J. W., Jr. *J. Chem. Phys.* **1988**, *88*, 922–935.

(29) Villà, J.; Truhlar, D. G. *Theor. Chem. Acc.* **1997**, *97*, 317–323.

(30) Eckart, C. *Phys. Rev.* **1930**, *35*, 1303–1309.

(31) Kassel, L. S. *J. Phys. Chem.* **1928**, *32*, 1065–1079.

(32) Dean, A. M. *J. Phys. Chem.* **1985**, *89*, 4600–4608.

(33) Chang, A. Y.; Bozzelli, J. W.; Dean, A. M. *Z. Phys. Chem.* **2000**, *214*, 1533–1568.

(34) Holbrook, K. A.; Pilling, M. J.; Robertson, S. H. *Unimolecular Reactions*; John Wiley & Sons, 1996.

(35) Wong, B. M.; Matheu, D. M.; Green, W. H., Jr. *J. Phys. Chem. A* **2003**, *107*, 6206–6211.

(36) Troe, J. *J. Phys. Chem.* **1979**, *83*, 114–126.

(37) Hippler, H.; Troe, J.; Wendelken, H. J. *J. Chem. Phys.* **1983**, *78*, 6709–6717.

(38) Carpenter, J. E.; Weinhold, F. *J. Mol. Struct. (Theochem)* **1988**, *169*, 41–62.

(39) Wolfe, S. *Acc. Chem. Res.* **1972**, *5*, 102–111.

(40) Brunck, T. K.; Weinhold, F. *J. Am. Chem. Soc.* **1979**, *101*, 1700–1709.

(41) Afeefy, H. Y.; Liebman, J. F.; Stein, S. E. Neutral Thermochemical Data. In *NIST Chemistry WebBook*; *NIST Standard Reference Database Number 69*; Linstrom, P. J., Mallard, W. G., Eds.; National Institute of Standards and Technology: Gaithersburg, MD, June 2005, p 20899; http://webbook.nist.gov.

(42) Peyerimhoff, S. D.; Skell, P. S.; May, D. D.; Buenker, R. J. *J. Am. Chem. Soc.* **1982**, *104*, 4515–4520.

(43) Feller, D.; Dixon, D. A.; Francisco, J. S. *J. Phys. Chem. A* **2003**, *107*, 1604–1617.

(44) Polanyi, J. C. *Acc. Chem. Res.* **1972**, *5*, 161–168.

(45) Weinhold, F.; Landis, C. R. *Valency and bonding: a natural bond orbital donor-acceptor perspective*; Cambridge University Press: New York, Cambridge, 2005.

(46) NIST Chemical Kinetics Database: Standard Reference Database 17, Version 7.0 (Web Version), Release 1.4; http://kinetics.nist.gov/kinetics/index.jsp (accessed in 2008).

(47) Atkinson, R.; Tuazon, E. C.; Aschmann, S. M. *Environ. Sci. Technol.* **2000**, *34*, 623–631.

JP8090792